

# Investigation of microstructure and V-defect formation in $\text{In}_x\text{Ga}_{1-x}\text{N}/\text{GaN}$ MQW grown using temperature-gradient MOCVD

M.C. Johnson<sup>a</sup>, Z. Liliental-Weber<sup>b</sup>, D.N. Zakharov<sup>b</sup>, D.E. McCready<sup>c</sup>,  
R.J. Jorgenson<sup>d</sup>, J. Wu<sup>a</sup>, W. Shan<sup>a</sup>, E. D. Bourret-Courchesne<sup>a\*</sup>

<sup>a</sup>Materials Sciences Division, Lawrence Berkeley National Laboratory, 1 Cyclotron Road, Mailstop 2R0200, Berkeley, CA 94720, USA

<sup>b</sup>Materials Sciences Division, Lawrence Berkeley National Laboratory, 1 Cyclotron Road, Mailstop 62R0203, Berkeley, CA 94720, USA

<sup>c</sup>Environmental Molecular Sciences Laboratory, Pacific Northwest National Laboratory, P.O. Box 999, MS K8-93, Richland, WA 99352, USA

<sup>d</sup>Oriol Inc., 3390 Viso Court, Santa Clara, CA 95054, USA

## Abstract

Temperature-gradient Metalorganic Chemical Vapor Deposition was used to deposit  $\text{In}_x\text{Ga}_{1-x}\text{N}/\text{GaN}$  multiple quantum well structures with a concentration gradient of indium across the wafer. These multiple quantum well structures were deposited on low defect density ( $2 \times 10^8 \text{ cm}^{-2}$ ) GaN template layers for investigation of microstructural properties and V-defect (pinhole) formation. Room temperature photoluminescence and photomodulated transmission were used for optical characterization which show a systematic decrease in emission energy for a decrease in growth temperature. Triple-axis X-ray diffraction, scanning electron microscopy and cross-section transmission electron microscopy were used to obtain microstructural properties of different regions across the wafer. Results show that there is a decrease in crystal quality and an increase in V-defect formation with increasing indium concentration. A direct correlation was found between V-defect density and growth temperature due to increased strain and indium segregation for increasing indium concentration.

*Keywords:* A1. Defects; A1. High resolution X-ray diffraction; A1: Transmission Electron Microscopy; A3. Metalorganic Vapor Phase Epitaxy; B1. Nitrides; B2. InGaN/GaN

## 1. Introduction

The deposition of high quality InGaN/GaN multiple quantum well (MQW) structures using Metalorganic Chemical Vapor Deposition (MOCVD) has become a very important industrial and commercial process. Blue/green light emitting diodes (LEDs) and laser diodes (LDs) using InGaN/GaN MQW structures are already commercially available with white LEDs emerging into production based on this technology [1, 2]. Although these nitride based devices have been very successful, the continued progress of depositing high quality materials for these LEDs is often limited by the lack of a fundamental understanding of InGaN/GaN MQW synthesis [3]. As demand for devices based on this technology increases, such as high brightness LEDs and low wavelength LDs, it is especially important that the fundamental issues for deposition of high quality  $\text{In}_x\text{Ga}_{1-x}\text{N}/\text{GaN}$  advanced structures be understood [4].

Optical properties of LEDs are directly related to film quality which is easily influenced by the fabrication processes and growth conditions. MOCVD is the method of choice although it poses many challenging issues. The growth of high quality InGaN/GaN MQW structures for the active layers of optoelectronic devices is very difficult due to the difference in the optimized growth temperatures between the InGaN well and the GaN barrier [5]. InN decomposes at approximately 550°C under a flow of  $\text{NH}_3$  and has a very low miscibility in GaN [6]. GaN is grown at temperatures greater than 1000°C to obtain an acceptable cracking efficiency of ammonia and high crystal quality. In order to compromise between these two extreme requirements the growth temperatures for  $\text{In}_x\text{Ga}_{1-x}\text{N}$  ( $0 < x < 1$ ) are chosen between 500°C- 800°C [7-9].

GaN films are known to contain a high density of microstructural defects due to the heteroepitaxial deposition on lattice mismatched substrates (usually sapphire or SiC). In addition, the difference in the thermal expansion coefficient between the GaN and the foreign substrate facilitates in high defect densities for the layer. These defects determine the crystal quality of the deposited layer which ultimately affects the optical and electrical performance of the material [10]. Forming a ternary alloy by the addition of indium in the layers increases the difficulty of obtaining high quality material. Local compositional variations within the ternary InGaN well [11, 12] lead to In segregation and the formation of In quantum dots [13, 14]. In addition, this In segregation on particular crystallographic planes leads to the formation of microstructural defects such as V-defects (pinholes) [15-20].

V-defect formation is commonly observed in InGaN/GaN heterostructures. A V-defect is an open hexagonal, inverted pyramid with six  $\{10\bar{1}1\}$  planes and a base on the (0001) c-plane [15, 21]. Thus, these defects appear as an open “V” in cross section transmission electron microscopy images. There are different reports on the origin of these defects. There are several reports showing that these pinholes are formed at different structural defects such as dislocations [22,23], stacking faults [24], grain boundaries [25], and inversion domains [26]. Theoretical work by Northup shows that accumulations of In on  $\{10\bar{1}1\}$  planes would lead to V-defect formation [21]. Those calculations considered that these defects need to be formed at dislocations where additional strain field at dislocation cores decrease the V-defect formation energy. The experimental work by Liliental-Weber *et al.* [15] postulates that impurities or dopants accumulate on  $\{10\bar{1}1\}$  planes decreasing

growth rate which leads to formation of V-defects [26, 27]. Wu *et al.* propose that V-defects in InGaN materials are formed due to In incorporation which hinders Ga incorporation [28]. Liu *et al.* show that In segregation in AlInGaN is responsible for V-defect formation and increased indium content leads to increased V-defect density [18]. Recent work by Florescu *et al.* [19] and Ting *et al.* [20] shows that V-defect formation in InGaN/GaN MQW structures may be caused by a combination of effects due to barrier growth temperature and the formation of In-rich regions within the quantum well under specific growth conditions.

In the present study, a growth method of temperature gradient MOCVD was used to investigate V-defect formation in  $\text{In}_x\text{Ga}_{1-x}\text{N}/\text{GaN}$  MQW structures. High quality  $\text{In}_x\text{Ga}_{1-x}\text{N}/\text{GaN}$  MQW structures were deposited on low defect GaN template layers by imposing a large temperature gradient across the substrate while holding all other growth parameters constant. This technique eliminates run-to-run variation allowing an accurate study of temperature effects on the deposition of these advanced structures. This deposition technique was utilized to investigate the microstructural properties as a function of growth temperature for the deposition of  $\text{In}_x\text{Ga}_{1-x}\text{N}/\text{GaN}$  MQW structures.

## **2. Experimental procedure**

$\text{In}_x\text{Ga}_{1-x}\text{N}/\text{GaN}$  MQW structures were grown on 2" (0001) sapphire substrates using a vertical flow EMCORE D180 MOCVD reactor. Trimethylgallium (TMG), Trimethylindium (TMI) and ammonia were used as the precursors for Ga, In, and N, respectively.  $\text{N}_2$  was used as the carrier and dilution gases for the deposition of both the

well and the barrier of the active InGaN/GaN (20Å/110Å, nominal) regions to increase the amount of In incorporation while H<sub>2</sub> was used for all other layers. A low temperature GaN nucleation layer was deposited at 550°C followed by an ~3µm thick, high temperature, low defect density (~2x10<sup>8</sup> cm<sup>-2</sup>) GaN template layer at 1050°C. This was followed by the growth of 7 periods of InGaN/GaN MQW structures with a temperature gradient across the wafer from 710°C at the cool end to 785°C at the hot end. The structure is capped by a final barrier layer of GaN which is approximately 100Å thick. The gradient was imposed by adjusting the power input to two resistive heaters that are placed under the susceptor at opposite ends of the substrate position. The temperatures at the end positions of the substrate were determined by IR pyrometry. Figure 1 shows a schematic of the substrate with temperature gradient. It is important to note that this reactor is capable of growing compositionally uniform In<sub>x</sub>Ga<sub>1-x</sub>N structures when a zero-temperature gradient is used.

Optical properties were analyzed using room temperature (RT) photoluminescence (PL) for emission output, and RT photo-modulated transmission (PT) spectroscopy for band edge transition. The photoluminescence signals were generated by excitation with the 325 nm line of a HeCd laser (~ 3 mW). The signals were then dispersed by a 1 m double-grating monochromator and detected by a Hamamatsu R928 photomultiplier tube. For photo-modulated transmission spectroscopy experiments, quasi-monochromatic light from a Xenon lamp dispersed by a 0.5 m monochromator was focused on the surface of samples polished on the back side as a probing beam. An ultra-violet enhanced Si photo-diode was used as the detector while a chopped HeCd laser beam provided the modulation.

Microstructural properties were analyzed using triple-axis X-ray diffraction (TAXRD) and

cross-section transmission electron microscopy (XTEM). The TAXRD data were collected using a Philips X'Pert Pro MRD system (PW3040/60 type) with a Cu X-ray source operated at 1.8 kW. The incident beam conditioner was hybrid-type that combined an X-ray mirror with a four-bounce Ge (220) crystal monochromator. The diffracted beam conditioner was a three-bounce Ge (220) analyzer crystal. The specimens were aligned on, and normalized to, the (0006) reflection of the sapphire substrate at  $2\theta = 41.680^\circ$  for the TAXRD measurements. To determine the sample microstructure dependence on growth temperature, cross-sectional samples for TEM analysis were prepared by mechanical polishing followed by ion milling. Thinned samples were examined using a JEOL 3010 transmission electron microscope operated at 300 kV. At least two samples from three different growth temperature regions (1,4, and 7) have been studied. Plan view images were taken using a high resolution FEI Sirion 200 Scanning Electron Microscopy (SEM) operated at 2kV.

### **3. Results and discussion**

#### *3.1. Optical Characterization*

Figure 2 shows the peak emission energy and the peak intensity taken for the RT photoluminescence results at seven equally spaced regions across the 2" wafer. PL raw data was previously reported [29]. Region 1 corresponds to a growth temperature of 785°C and Region 7 corresponds to a growth temperature of 710°C. The regions between these endpoints are assumed to have a linear temperature change with position (See Figure 1). The data show that there is a systematic evolution of PL emission across the wafer due to the imposed growth temperature gradient. The high temperature end (Region 1)

corresponds to the high energy emission. The peak PL emission energy decreases with decreasing growth temperature. There is a much greater change in the intensity of the main PL emission for the regions in the low temperature range (Region 5-7) than for the regions in the high temperature range (Regions 1-4). PL intensity is very large and relatively constant for this high temperature region while there is a large decrease in PL intensity as growth temperature decreases. The optical properties degrade rapidly for material deposited at growth temperatures below  $\sim 750^{\circ}\text{C}$ .

Figure 3 shows the indium concentration as a function of position across the wafer derived from previously reported PT data [29]. PT data determines the ground-state inter-band transition energies. These energies can be used in the standard equation determined by Wu *et al.* [30], which neglects quantum confinement and strain effects, to obtain indium concentrations for each region. Although the indium concentration is very difficult to obtain accurately, these experiments show that there is a definitive concentration gradient as a result of the growth temperature gradient.

### 3.2. *X-Ray Diffraction*

The indium concentrations were also determined from simulations using dynamic theory and fitted to the x-ray diffraction data. These results also show that there is an increase in indium content for a decrease in growth temperature. The In concentrations obtained using this technique were similar to those shown in Figure 3. Figure 4(a-c) show the TAXRD spectra for region 1, 4, and 7. The many and well-resolved satellite peaks indicate high-quality InGaN/GaN MQW structures. But for subsequent regions, these spectra show that

there is a decrease in the number of these satellite peaks in addition to systematic broadening which indicates a decrease in crystal quality. Degradation of crystal quality is observed when growth temperature decreases from 785°C to 710°C for which indium concentrations are increasing across the wafer. A clear shift of the  $\text{In}_x\text{Ga}_{1-x}\text{N}$  peak (marked by the arrow in Figure 5) located on the low angle side of the GaN (0002) peak is observed. A shift in the  $\text{In}_x\text{Ga}_{1-x}\text{N}$  peak to lower diffraction angles is due to the increase in lattice spacing caused by the increased indium incorporation. This result verifies the increase in indium concentration across the wafer that was observed in the optical characterization (Figures 2 & 3). Additionally, the number of superlattice peaks decreases and their width increases with decreasing deposition temperature which implies that the crystal quality of the corresponding region qualitatively decreases with decreasing growth temperature.

Figure 5 also shows an expanded plot of the TAXRD data as a function of position (temperature) for  $2\theta$  diffraction angles of 33-35 degrees. The program Philips X'Pert Epitaxy 4.0 was used for analysis on the three superlattice fringes on the low angle side of the GaN (0002) peaks. Analysis resulted in a superlattice thickness (InGa $\text{N}$  well and Ga $\text{N}$  barrier) of 126 Å, 140 Å, and 169 Å, for regions 1, 4, and 7, respectively, which is in good agreement with the XTEM measurements discussed below.

### 3.3. TEM and SEM Characterization

Figure 6 shows bright field XTEM images of the MQW areas for regions 1, 4, and 7. Region 1 (Figure 6a) contains the smallest number of V-defects ( $1.0 \times 10^{10} \text{ cm}^{-2}$ ) and shows very sharp interfaces between the wells and barriers. In this region, the V-defects are

shallow and extend into the superlattice structure approximately 150 Å below the sample surface. Region 4 (Figure 6b) also exhibits very clean interfaces, but the V-defect density increases to approximately  $1.5 \times 10^{10} \text{ cm}^{-2}$ . These defects extend into the MQW region approximately 300 Å (approximately the 3 top superlattice layers) below the sample surface. Region 7 (Figure 6c) has a V-defect density approximately  $5.0 \times 10^{10} \text{ cm}^{-2}$ . The top three superlattice layers are heavily corrugated and completely destroyed for most of this low temperature (710°C) grown material. In some locations, indicated by arrows labeled 2, 5 and 6 in Figure 6c, V-defects can extend all the way through the entire MQW area. Table 1 summarizes the results of our present studies.

High Resolution Scanning Electron Microscopy (SEM) was also performed to verify and obtain information on V-defect formation properties. Figure 7 shows a typical plan-view image taken from region 1 of the sample. This image shows grain boundaries (GB) decorated by V-defects which overlap each other. It also shows single V-defects (indicated by arrows) which are probably formed in dislocation free areas or at single dislocations originated in the GaN template layer. These V-defects have the characteristic hexagonal shape and a diameter ranging from 200-250 Å which is consistent with measurements from the TEM images for region 1.

#### **4. Discussion**

Several groups have found that V-defects in InGaN material can be caused by threading dislocations from the GaN template layer [21, 23]. Our earlier studies show that for constant In composition in the samples consisting of 5 quantum wells, V-defects are

formed only at some dislocations. But when the number of quantum wells is increased to 20 while containing the same In composition there is an increase in V-defect density where these V-defects are formed at all dislocation sites and also in areas free of dislocations [31]. The InGaN/GaN layers discussed here were grown on a GaN template layer with a dislocation density as low as  $2 \times 10^8 \text{ cm}^{-2}$ . Since the same template was used for the growth of the MQW layers we could show a constant dislocation density across the wafer which is verified from the TEM results. However, density of V-defects increases across the wafer. This increase is consistent with the increase in In content. It is also shown that the density of V-defects is almost two orders of magnitude higher when compared to the density of threading dislocations. Therefore, threading dislocations sites cannot be the only location of V-defect formation. Our present X-ray diffraction results and previous studies [32] show that decreasing the growth temperature of InGaN leads to higher indium concentrations in these layers. Based on these results, it is clear that the density of V-defects in the InGaN layers is proportional to the indium concentration in the respective regions (1-7) of the sample. This confirms earlier work of Liliental-Weber that V-defect density increases with impurity or dopant concentration and it is not necessarily associated with threading dislocation density [12, 27].

For material containing higher indium content, the indium accumulation near threading dislocations or on strained-relieved  $\{10\bar{1}1\}$  planes starts at the first InGaN well and leads to earlier V-defect nucleation than for structures having lower indium content. These V-defects formed due to early accumulation propagate and expand through the subsequent layers as the InGaN/GaN MQW structures are deposited. This ultimately results in larger

geometric size of V-defects on the sample surface for layers containing higher indium content. Figure 8 shows the relationship between increasing V-defect density and decreasing optical performance. The association of size and density of V-defects with increased In content is therefore detrimental to device application. The decrease in optical performance at growth temperatures below  $\sim 750^{\circ}\text{C}$  is believed to be directly related to the increase in V-defect density.

## **5. Conclusion**

Temperature-gradient MOCVD was used to grow compositionally graded  $\text{In}_x\text{Ga}_{1-x}\text{N}/\text{GaN}$  MQW structures to investigate the effect of indium incorporation on microstructural properties. Optical characterization and TAXRD results showed a systematic increase in indium concentration and decrease in crystal structure quality with a decrease in growth temperature. Using TEM and SEM we showed that the density of V-defects systematically increases with the increase in indium concentration. Since the same template was used with a constant dislocation density, we could conclude that V-defects were formed not only at dislocation sites but also in the dislocation free areas. Growth conditions to limit this V-defect formation, especially for high In content materials, is currently being investigated.

## **Acknowledgement**

This work was supported by the Director, Office of Science, Office of Basic Energy Sciences, Division of Materials Science and Engineering, of the U.S. Department of Energy under Contract No. DE-AC03-76SF00098. The use of facilities at the National Center for Electron Microscopy was greatly appreciated. The research described in this paper was performed in part in the Environmental Molecular Sciences Laboratory, a national scientific user facility sponsored by the US Department of Energy's Office of Biological and Environmental Research and located at Pacific Northwest National Laboratory in Richland, WA.

## References

1. M. Yamada, Y. Narukawa, T. Mukai, Jap. J. Appl. Phys. 41(3a)(2002)L246.
2. Y.C. Shen, J.J. Wierer, M.R. Krames, M.J. Ludowise, M.S. Misra, F. Ahmed, A.Y. Kim, G.O. Mueller, J.C. Bhat, S.A. Stockman, P.S. Martin, Appl. Phys. Lett. 82(2003)2221.
3. C.H. Liu, Y.K. Su, T.C. Wen, S.J. Chang, R.W. Chuang, J. Crystal Growth 254(2003)336.
4. U. Kaufman, M. Kunzar, K. Kohler, H. Obloh, W. Pletschan, P. Schlotter, J. Wagner, A. Ellens, W. Rossner, M. Kobusch, Phys. Stat. Solid. (a) 192(2002)246.
5. Sunwoon Kim, Kyuhan Lee, Keunseop Park and Chang-Soo Kim, J. Crystal Growth 247(2003)62.
6. I.H. Ho, G.B. Stringfellow, Appl. Phys. Lett. 69(1996)2701.
7. A. Yamamoto, M. Adachi, A. Hashimoto, J. Crystal Growth 230(2001)351.
8. E.J. Thrush, M.J. Kappus, P. Dawson, M.E. Vickers, J. Bernard, D. Girgham, G. Makaronidis, F.D.G. Rayment, L. Considine, C.J. Humphreys, J. Crystal Growth 248(2003)518.
9. S.N. Lee, T. Sakong, L. Wonseok, H. Pack, M. Seon, I.H. Lee, O. Nam, Y. Park, J. Crystal Growth 250(2003)256.
10. T.L. Song, S.J. Chua, E.A. Fitzgerald, P. Chen, S. Tripathy, Appl. Phys. Letts. 83(2003)1545.
11. M.C. Johnson, E.D. Bourret-Courchesne, J. Wu, Z. Liliental-Weber, D.N. Zakharov, R.J. Jorgenson, T.B. Ng, D.E. McCready, J.R. Williams, J. Appl. Phys. (accepted, 2004).
12. Z. Liliental-Weber, M. Benamara, J. Washburn, J.Z. Domagala, J. Bak-Misiuk, E.L. Piner, J.C. Roberts, S.M. Bedair, J. Elec. Mats. 30(2001)439.
13. I. Ho, G.B. Stringfellow, Appl. Phys. Lett. 69(1996)2701.
14. A. Hangleiter, F. Hitzel, S. Lahmann, U. Rossow, Appl. Phys. Lett. 83(2003)1169.
15. Z. Liliental-Weber, S. Ruvimov, W. Swider, Y. Kim, J. Washburn, S. Nakamura, R.S. Kern, Y. Chen, J.W. Yang, MRS Symposium Proceedings 482(1998)1375.

16. S.M. Ting, J.C. Ramer, D.I. Florescu, V.N. Merai, B.E. Albert, A. Parekh, D.S. Lee, D. Lu, D.V. Christini, L. Liu, E.A. Armour, *J. Appl. Phys.* 94(2003)1461.
17. H.K. Cho, J. Y. Lee, C.S. Kim, G.M. Yang, N. Sharma, C. Humphreys, *J. Crystal Growth* 231(2001)466.
18. J.P. Liu, Y.T. Wang, H. Yang, D.S. Jiang, U. Jahn, K.H. Ploog, *Appl. Phys. Lett.* 84(2004)5449.
19. D.I. Florescu, S.M. Ting, J.C. Ramer, D.S. Lee, V.N. Merai, A. Parkeh, D. Lu, E.A. Armour, L. Chernyak, *Appl. Phys. Lett.* 83(2003)33.
20. S.M. Ting, J.C. Ramer, D.I. Florescu, V.N. Merai, B.E. Albert, A. Parekh, D.S. Lee, D. Lu, D.V. Christini, L. Liu, E.A. Armour, *J. Appl. Phys.* 94(2003)1461.
21. J.E. Northrup, L.T. Romano, J. Neugebauer, *Appl. Phys. Lett.* 74(1999)2319.
22. Y. Chen, T. Takeuchi, H. Amano, I. Akasaki, N. Yamada, Y. Kaneko, S.Y. Wang, *Appl. Phys. Lett.* 72(1997)710.
23. P.Q. Miraglia, E.A. Preble, A.M. Roskowski, S. Einfeldt, R.F. Davis, *J. Crystal Growth* 253(2003)16.
24. H.K. Cho, J.Y. Lee, G.M. Yang, C.S. Kim, *Appl. Phys. Lett.* 79(2001)215.
25. M.G. Cheong, E.K. Suh, H.J. Lee, M. Dawson, *Semicond. Sci. Technol.* 17(2002)446.
26. Z. Liliental-Weber, Y. Chen, S. Ruvimov, J. Washburn, *Phys. Rev. Lett.* 79(1997)2835.
27. Z. Liliental-Weber, *J. Electron Microscopy* 49(2000)339.
28. X.H. Wu, C.R. Elsass, A. Abare, M. Mack, S. Keller, P.M. Petroff, S.P. DenBaars, J.S. Speck, S.J. Rosner, *Appl. Phys. Lett.* 72(1997)692.
29. M.C. Johnson, R.J. Jorgenson, J. Wu, W. Shan, E. Bourret-Courchesne, *J. Crystal Growth* 261(2004)44.
30. J. Wu, W. Walukiewicz, K.M. Yu, J.W. Ager III, E.E. Haller, H. Lu, W.J. Schaff, *Appl. Phys. Lett.* 80(2002)4741.
31. Z. Liliental-Weber, S. Ruvimov, W. Snider, Y. Kim, J. Washburn, S. Nakamura, R.S. Kern, Y. Chen, J.W. Yang, *Mat. Res. Soc. Symp. Proc.* 482(1998)375.
32. S. Keller, S.P. DenBaars, *J. Crystal Growth* 248(2003)479.

## Table and Figure Captions

**Table 1** – Comparison of microstructural properties for different regions of wafer. V-defect density increases with an increase in indium concentration.

**Figure 1** – Schematic of temperature gradient imposed by varying input power to two electrical heaters located at the ends of the substrate. Temperature gradient is assumed to be linear with Region 1 measured to be 785°C and Region 7 measured to be 710°C.

**Figure 2** – PL peak emission energy and PL intensity as a function of position/temperature across the wafer.

**Figure 3** – Calculated indium concentration in each region using observed bandgaps from PT experiments [26]. Indium concentration,  $x$ , was calculated using standard equation determined by Wu *et al.* [27]. Concentrations were verified using XRD analysis.

**Figure 4** – TAXRD spectra for (a) region 1, (b) region 4, and (c) region 7. The sharp peak at 34.5 degrees is due to diffraction from GaN (0002).

**Figure 5** – Expanded scale and offset overlay of TAXRD spectra for regions 1, 4, and 7. The arrows indicate diffracted peak from the  $\text{In}_x\text{Ga}_{1-x}\text{N}$  layer which shift to smaller angles due to increased lattice spacing.

**Figure 6** - XTEM images of  $\text{In}_x\text{Ga}_{1-x}\text{N}/\text{GaN}$  MQW for regions 1, 4, and 7. V-defect density increases with a decrease in growth temperature. Region 7 shows that these defects completely destroy the top layers of the structure.

**Figure 7** – Typical plan view SEM image of region 1. V-defects are shown to cover surface in dislocation free areas as well as on grain boundaries (GB). This image shows size of V-defects and its characteristic hexagonal shape.

**Figure 8** – Relationship between V-defect density and optical quality as a function of indium concentration. Optical quality decreases as V-defect density increases.

**Table 1**

| <b>Region</b> | <b>T<sub>g</sub> (°C)</b> | <b>x for<br/>In<sub>x</sub>Ga<sub>1-x</sub>N</b> | <b>V-defect<br/>Density<br/>(x10<sup>10</sup> cm<sup>-2</sup>)</b> | <b>Diameter of<br/>V-defects at sample<br/>surface (nm)</b> | <b>Maximum<br/>Depth of<br/>V-defects (Å)</b> |
|---------------|---------------------------|--|--|---|---|
| <b>1</b>      | <b>785</b>                | <b>0.09</b>                                      | <b>1.0</b>   | <b>15 - 30</b>  | <b>150</b>                                    |
| <b>4</b>      | <b>747</b>                | <b>0.16</b>                                      | <b>1.5</b>   | <b>50 - 80</b>  | <b>300</b>                                    |
| <b>7</b>      | <b>710</b>                | <b>0.32</b>                                      | <b>5.0</b>   | <b>50 - 170</b>   | <b>600</b>                                    |

Figure 1

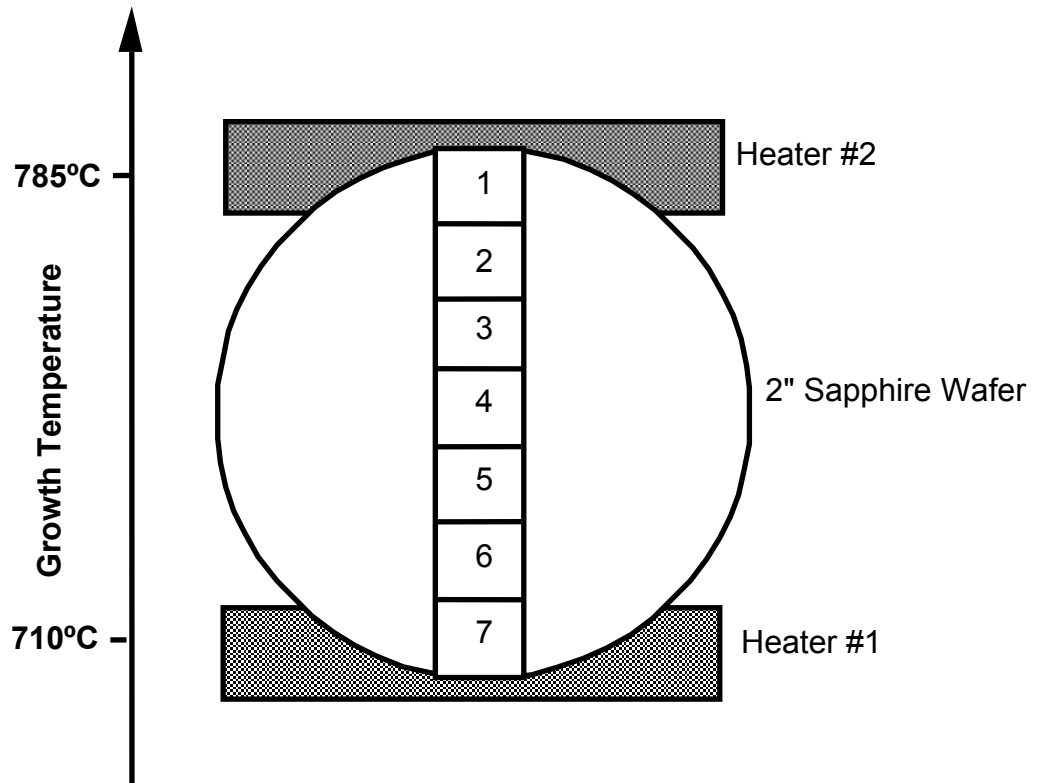


Figure 2

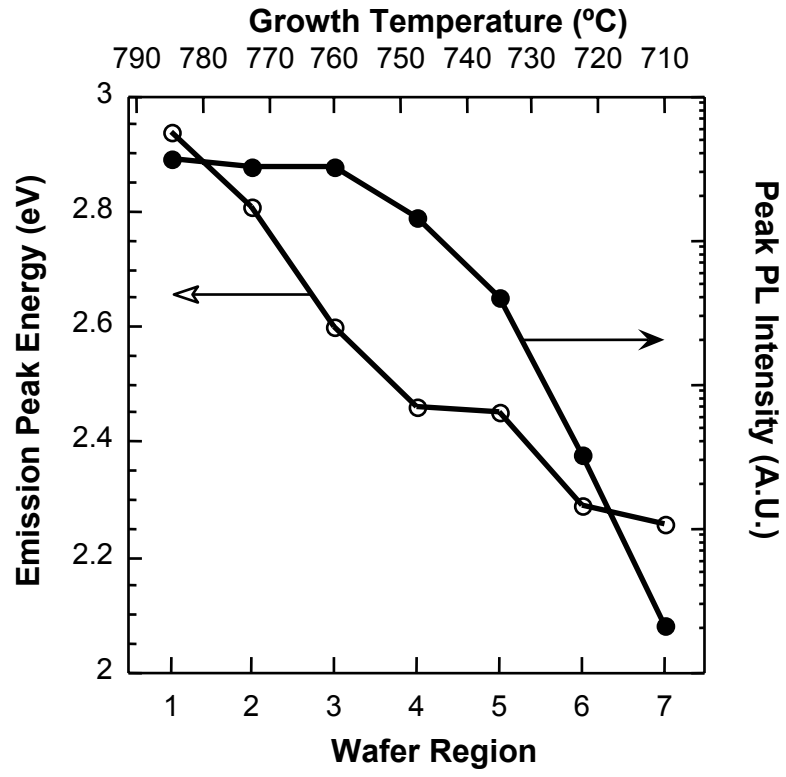
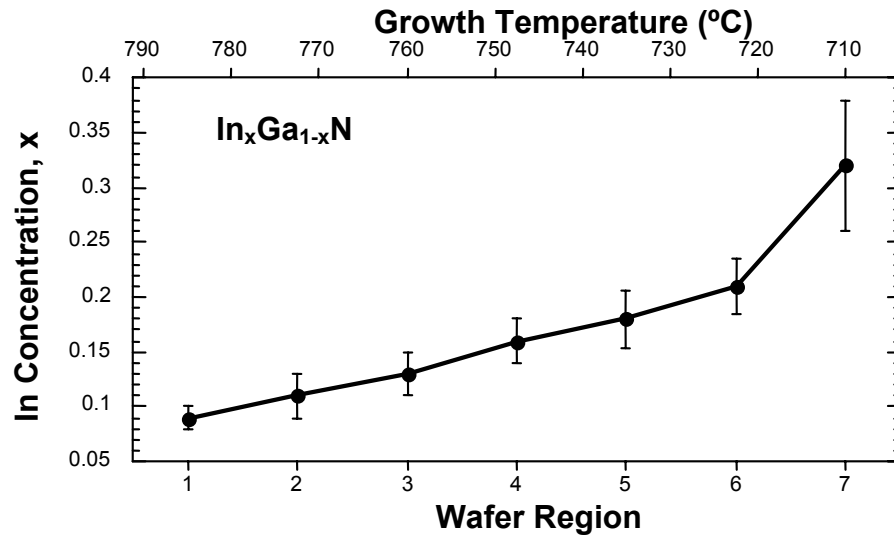


Figure 3



**Figure 4**

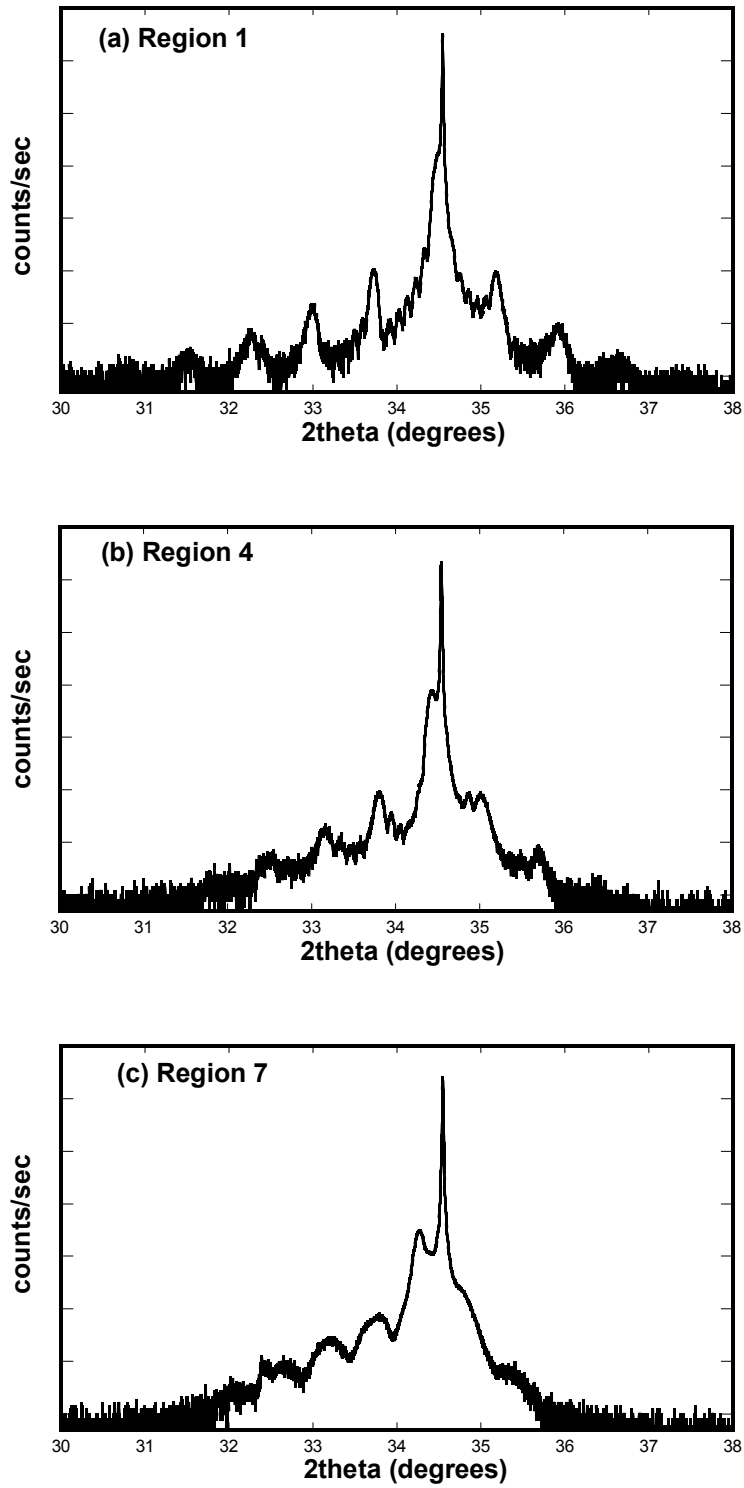


Figure 5

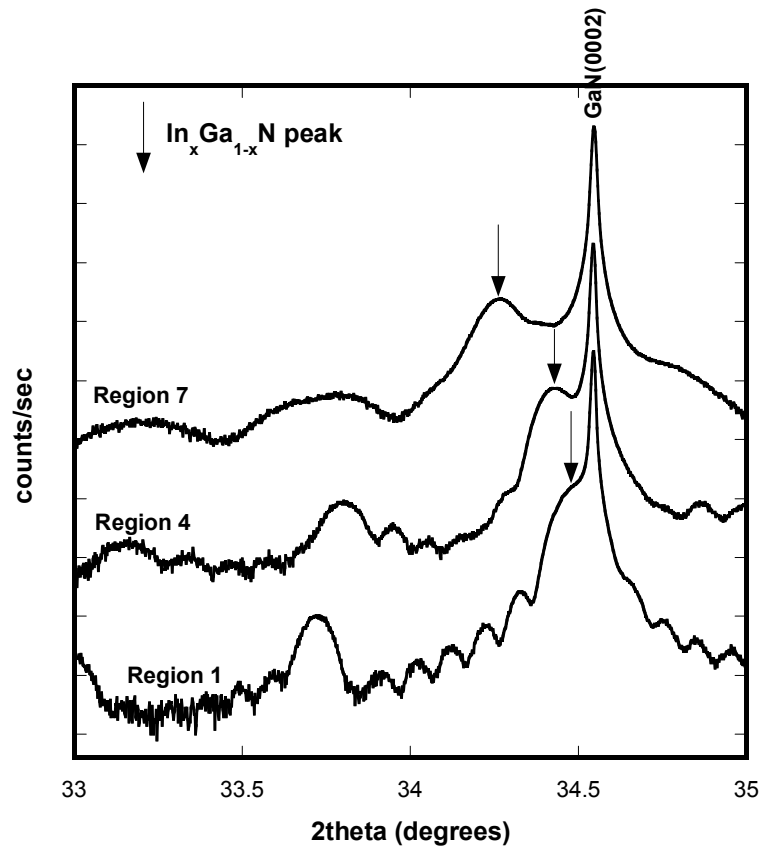
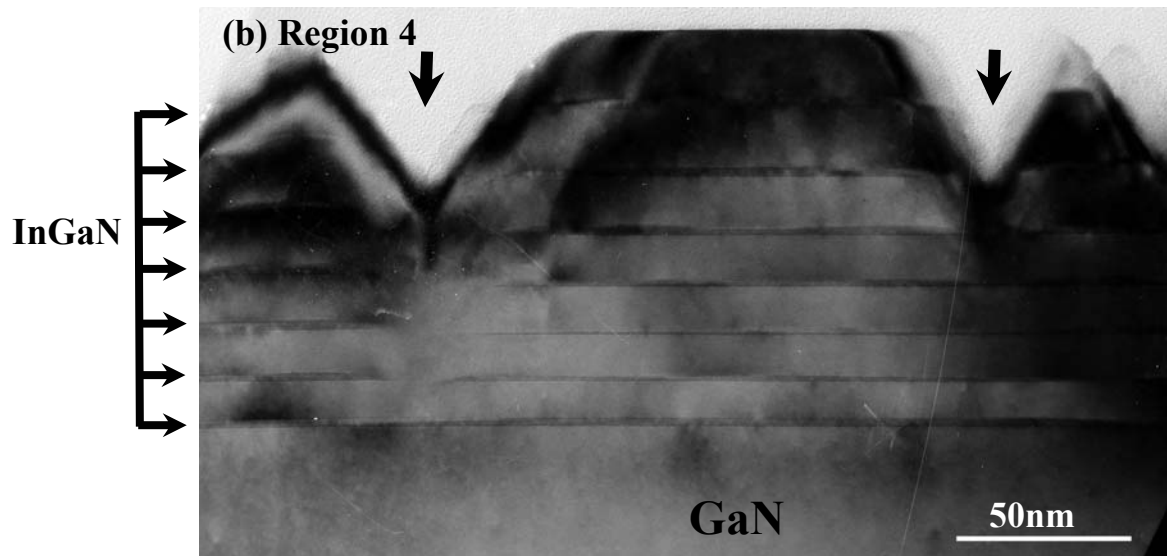
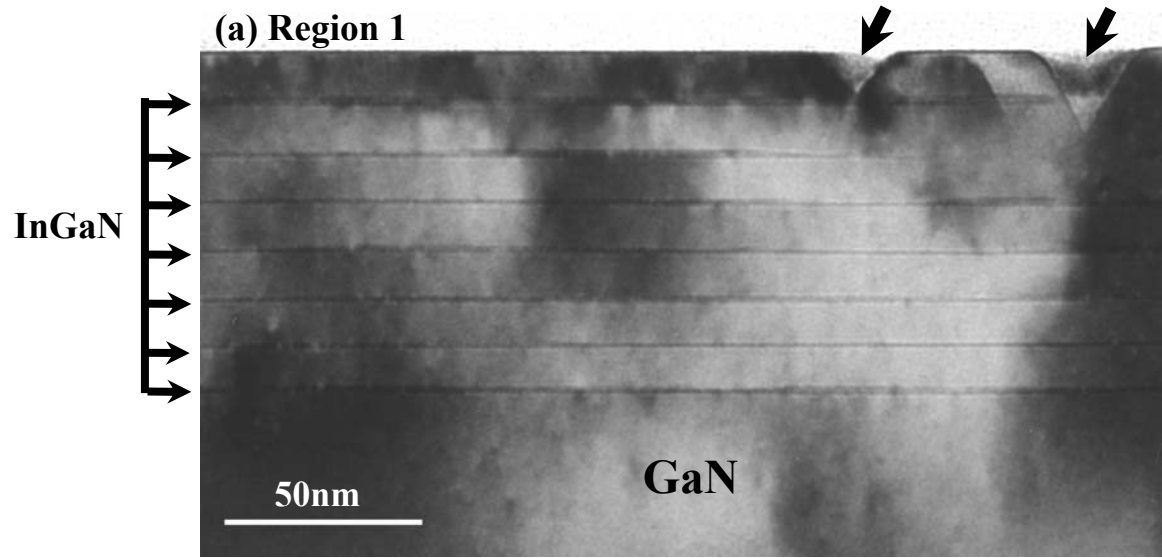
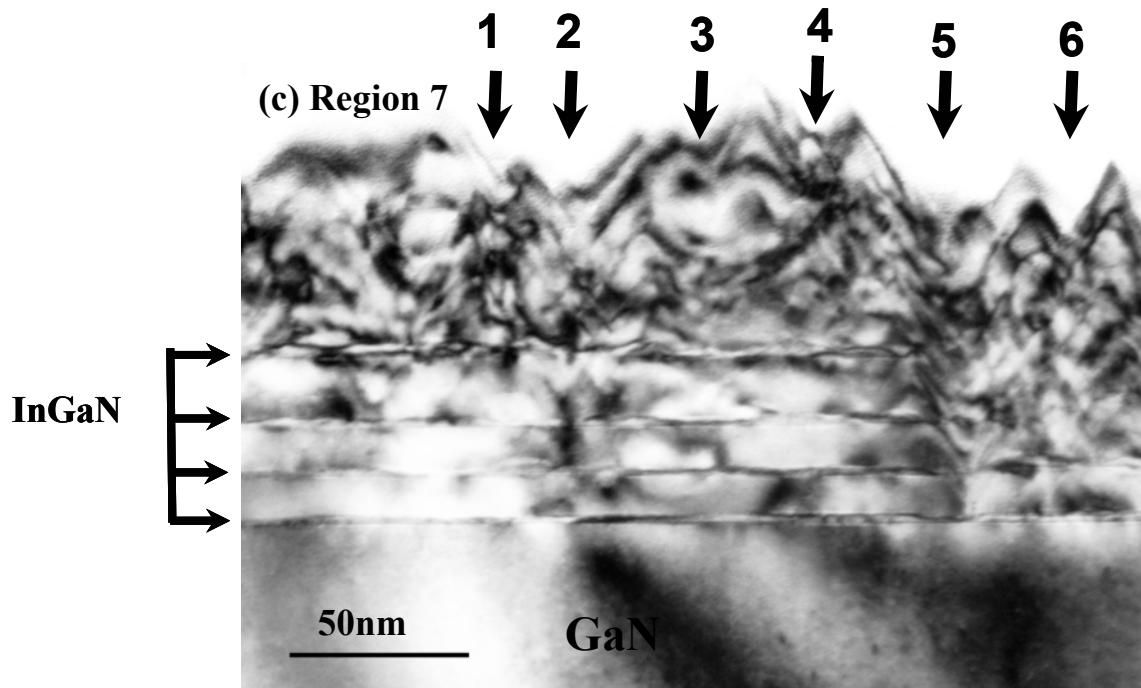


Figure 6





**Figure 7**

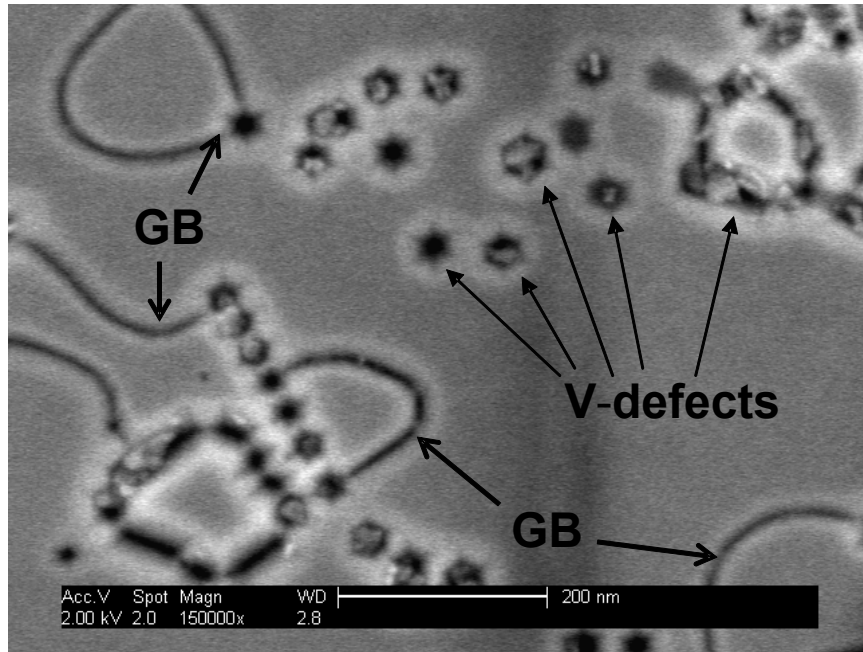


Figure 8

